Environmental and Climate Technologies
2025, vol. 29, no. 1, pp. 1073–1091
https://doi.org/10.2478/rtuect-2025-0072
https://content.sciendo.com

1862
RIGA TECHNICAL UNIVERSITY

Hydrothermal Humification of Extracted Spruce Greenery Biomass as a Tool for End-of-Waste Approach for Production of Artificial Humic Substances

Lauris ARBIDANS[1*], Marcis MEZULIS[2], Linda DOBKEVICA[3], Andris ANTUZEVICS[4]
Arturs ZARINS[5], Maris KLAVINS[6]

[1–3,6]*Department of Environmental Science, University of Latvia, Raina Blvd. 19, Riga, LV-1586, Latvia*

[4]*Institute of Solid State Physics, University of Latvia, Kengaraga 8, LV-1063 Riga, Latvia*

[5]*Institute of Chemical Physics, Faculty of Science and Technology, University of Latvia, Jelgavas 1, LV-1004, Riga, Latvia*

[5]*Department of Environment and Technologies, Faculty of Natural Sciences and Healthcare, Daugavpils University, Parades 1A, LV-5401, Daugavpils, Latvia*

Received 19.03.2025; accepted 11.12.2025

***Abstract* – Forestry sector produces a considerable amount of underutilised biowaste that can be valorised into high added value products. A prospective material is Norway spruce branches and needles, also known as spruce greenery. This study is a follow up from a previously explored green chemistry application of conifer greenery extraction, using green solvents. After extraction, a significant amount of spruce lignocellulose waste is produced, that can be thermochemically converted to artificial humic substances that mimic the properties of natural humic substances. The proposed technology is hydrothermal humification, which is considered to be climate neutral, as it produces no greenhouse gas emissions during the process. This study focuses on hydrothermal humification process application on extracted spruce greenery lignocellulose waste. Reaction conditions have been evaluated, to achieve the highest product yield, while maintaining least energy consumption possible, and the conditions were found to be 185 °C and 9 hours. Reaction byproducts have been identified, such as carbohydrates and polyphenol-like structures and their dynamics depending on reaction conditions. Contemporary methods have been applied to investigate the formation and structure of artificial humic acids. UV-Vis, FTIR and solid-state ^{13}C NMR revealed that higher reaction temperatures increase the aromaticity and robustness of said humic acids, however, applying temperatures over 200 °C promotes the formation of potentially harmful free radicals, proven by EPR spectroscopy.**

***Keywords* – Bioeconomy; biowaste; HTH; humic acid; Norway spruce; peat; valorisation.**

Nomenclature	
AHA	Artificial humic acid
EPR	Electron paramagnetic resonance
GHG	Greenhouse gas

* Corresponding author.
E-mail address: lauris.arbidans@lu.lv

HTH	Hydrothermal humification
SFS	Synthetic fulvic acid solution

1. INTRODUCTION

There is a clear need to replace fossil resources with renewable ones to reduce the depletion of non-renewable or slowly renewable resources and combat climate change. One solution for limiting fossil resource use is the development of a bioeconomy based on biomass waste, which can be considered a sustainable approach [1]. The European Green Deal (EGD) aims to reduce greenhouse gas (GHG) emissions by at least 55 % by 2030 compared to 1990 levels and make Europe the first climate-neutral continent by 2050. At the same time, the EGD also aims to significantly reduce peat extraction for low-value products like fuel or soil enhancers [2], encouraging alternative methods for obtaining soil improvement agents.

Peat is currently the main raw material for soil enhancers, but it is a non-renewable fossil resource, and its extraction produces significant GHG emissions, mainly CO_2 and CH_4, with some N_2O. According to the Latvian State Forest Research Institute "Silava," 70 % of peat's GHG emissions come from agricultural peat, 16 % from degraded land, 9 % from active or recently closed peat extraction sites, and 5 % from renaturalised areas, with total GHG emissions amounting to 1709 kt CO_2 equivalent [3].

A potential alternative material for soil enhancer production is forest waste, such as spruce greenery, which are left behind after logging. This biomass, which can make up to 50 % of tree dry weight, can be processed thermochemically into soil enhancers or artificial humic substances through hydrothermal humification [4], [5]. By valorising this biomass waste, circular economy principles are promoted, GHG emissions are reduced, and the depletion of slowly renewable resources is mitigated, while also producing soil enhancers.

This study is an end-of-waste approach to our previous study [6] that focuses on green chemistry and extraction of spruce greenery, after which a lignocellulose biomass waste is produced that can be valorised further. According to previous study, approximately 10 % of total extractives per dry weight of said spruce greenery can be obtained, which leaves a significant amount of lignocellulose waste.

Hydrothermal humification (HTH) is a form of hydrothermal carbonization performed in an alkaline environment KOH as a catalyst, significantly accelerating natural humification – up to 10^9 times faster – while ensuring high carbon retention in the final product, unlike pyrolysis, which leads to substantial CO_2 and CO emissions, therefore this technology can be considered climate-neutral [7]. Hydrothermal humification is typically conducted in sub-critical water in a temperature range of 150–250 °C with self-generated pressure in a closed environment.

Several process parameters play a crucial role in determining reaction pathways and product characteristics. Temperature directly influences reaction kinetics, as higher temperatures accelerate depolymerization and subsequent condensation reactions, though excessively high temperatures may lead to unwanted carbon residue formation, reducing humic acid yield [8]. Pressure affects the solubility of reactants and intermediates, with higher pressure enhancing molecular interactions and reaction efficiency [9]. KOH concentration is another key factor, as higher concentrations promote depolymerization by providing more hydroxide ions to cleave glycosidic and ester bonds; however, excessively high concentrations can degrade monomers, leading to lower overall yields [10].

The composition of the biomass feedstock also significantly impacts HTH efficiency and product quality. Biomasses with high lignin content require more severe hydrothermal conditions, such as higher temperatures and longer synthesis times, to achieve effective depolymerization, whereas cellulose-rich biomass can be processed under milder conditions, often yielding higher amounts of artificial humic substances [11], [12]. According to literature [13], spruce wood consists of mainly 40–44 % cellulose, 25–29 % hemicellulose and 25–31 % lignin, which can be approximated to the needle and branch biomass (greenery) used in this study and the greenery is a suitable lignocellulosic source to produce artificial humic substances.

The aim is to understand the possibilities of applying HTH technology on extracted spruce greenery biomass (a mix of needles and branches), using contemporary physico-analytical methods must be applied, such as UV-Vis; FTIR and EPR spectrometry, as well as ^{13}C-CPMAS-NMR to characterise the formation of artificial humic acids (AHAs) and investigate the dynamics of the process itself. Artificial humic acids are the primary HTH product, which have been intensively studied, while the solutions of low-molecular-weight by-products that form together with fulvic acids and their dynamics have been studied less. However, given the significant carbon transfer occurring in these solutions during HTH process, it is important to understand which intermediates or byproducts remain after synthesis, as well as their dynamics and structural composition, considering that fulvic acids and other low-molecular-weight substances are the second major product, as well as investigate the parameters that influence AHA formation and their structural characteristics, based on HTH parameters.

2. MATERIALS AND METHODS

2.1. Materials

Solvents: methanol, isopropanol (*Sigma-Aldrich*, Germany), ethanol (*z/s Jaunpēternieki*). Reagents and standards: HCl (37 %), $NaHCO_3$ (p.a.) and H_2SO_4 (≥97 %) purchased from *Enola*, Latvia, Na_2CO_3 (99.8 %, *Chempur*), KBr (p.a., *SpectrosoL*®), Neocuproine (p.a. *Merck*), $FeCl_3 \cdot 6H_2O$ (≥ 99 %, *Arcros-Organics*), KOH (p.a.), 2.2-diphenyl-1-picrylhydrazyl (p.a.), phenol (≥ 99 %), Folin-Ciocalteu reagent (FC reagent, 2 M), gallic acid (≥99 %), Trolox (97 %), 2,4,6-Tris(2-pyridyl)-*S*-triazine (TPTZ, ≥98 %), $CuCl_2$ (99 %), sodium acetate (≥99 %), ammonium acetate (≥ 98 %), D-glucose (≥99 %) purchased from *Sigma-Aldrich*, Germany.

2.2. Biomass Pre-treatment

Spruce (*Picea abies*) greenery (needles and branches) material was sampled in August 2023 near Aglona train station (Latvia, Lat. 56.166106, Long. 26.829501). After harvesting, spruce greenery was transported to the laboratory and dried at 45 ℃ (48 h) in a laboratory drying oven (*Gallenkamp Plus II*, United Kingdom). After drying, the greenery was ground in a laboratory mill (*Fritsch*, Germany), separated by particle size (<2 mm) and extracted 3 times with isopropanol, using ultrasonic rod (*Vibra Cell VCX 1500*, SONICS, USA) to obtain near fully extracted biomass that would mimic the final waste product after applying green chemistry to the spruce greenery [6]. After extraction with isopropanol, the greenery biomass that consisted of spruce needles and branches in a w/w% ratio of 4:1 was dried at 105 ℃ for 24 hours in a laboratory drying oven.

2.3. Hydrothermal Humification of Spruce Greenery Biomass

Based on previous research on HTH optimization [14], five synthesis treatment times were selected: 2, 4, 9, 14, and 24 hours, under six temperature conditions: 155, 170, 185, 200, 215, and 230 °C. Approximately 3 g of dried extracted spruce greenery was weighed on an analytical balance, quantitatively transferred to a 100 mL Teflon (PTFE) autoclave, and mixed with 50 mL of 0.65 M KOH solution. The autoclave was then placed in a pressure-resistant steel casing and sealed. The sample was heated at the selected temperature and duration in a laboratory drying oven (*Gallenkamp Plus II*). After synthesis, once the autoclave had cooled to room temperature, it was opened, the entire contents were filtered through filter paper, and the filtrate was collected for further analysis. Each synthesis was performed in triplicate.

2.4. Artificial Humic Substance Yield Analysis

Using a 15 mL Mohr pipette, the synthesized humic substance filtrate was quantitatively transferred to a 100 mL Erlenmeyer flask, and 1 mL of concentrated hydrochloric acid was added. The sample was mixed and allowed to stand for 10 minutes. The precipitated artificial humic acids were then filtered through filter paper, and the filtrate was collected for further analysis. The separated AHAs were washed with deionized water until a neutral pH was reached and then dried.

Using a 1000 µL automatic pipette, 500 µL of the total artificial humic substance solution is quantitatively transferred to a 100 mL volumetric flask. Separately, 500 µL of the isolated fulvic acids and low-molecular-weight compound solution (hereinafter referred to as the synthetic fulvic acid solution – SFS) is transferred to another 100 mL volumetric flask and diluted to the mark with deionized water. The diluted solutions were analysed using a total carbon analyser (*Shimadzu TOC-V_{CSN}*, Japan), and the results were calculated as milligrams of organic carbon transferred to liquid phase per gram of biomass hydrothermally humified. The carbon content of AHA was calculated by subtracting the SFS carbon concentration from the total fraction carbon content.

2.5. Physico-Chemical Characterisation of Artificial Humic Acids

Molecular Absorption Spectra (UV-Vis): a total of 20 mg of isolated and purified artificial humic acid was weighed using an analytical balance, quantitatively transferred to a 1 L volumetric flask, and dissolved in a 0.5 M $NaHCO_3$ solution. The solutions were measured in a 1 cm quartz cuvette using a UV-Vis spectrophotometer (UV-1800) in the range of 220 to 700 nm with a resolution of 1 nm. To characterize the AHA chromophore groups and assess humification degree, absorption ratios at wavelengths of 254 nm (E_2), 365 nm (E_3), 465 nm (E_4), and 665 nm (E_6) were calculated and expressed as E_2/E_3, E_2/E_4, E_2/E_6, and E_4/E_6.

Fourier Transform Infrared Spectroscopy (FTIR): before analysis, KBr was dried at 105 °C for 2 hours. Then, 200 mg of KBr was weighed, mixed with 2 mg of humic acid, and homogenized. The mixture was pressed into a pellet and measured using an FTIR spectrometer (Shimadzu IR-Tracer 100) in the range of 4000 cm^{-1} to 400 cm^{-1} with a resolution of 8 cm^{-1}, performing 16 scans.

Room-temperature EPR: measurements were carried out using a Bruker ELEXSYS-II E500 CW-EPR spectrometer operating at a microwave frequency of 9.834 GHz and power ranging from 1 to 100 mW, with a magnetic field modulation amplitude of 0.1 mT at 100 kHz. Signal intensities were normalised to sample mass. EPR spectra simulations were performed using EasySpin software [15].

Carbon-13 Cross-Polarization Magic Angle Spinning Nuclear Magnetic Resonance (^{13}C-CPMAS-NMR): the ^{13}C-CPMAS-NMR spectra were obtained at the Latvian Institute of Organic Synthesis using an 800 MHz Bruker Avance III HD spectrometer equipped with a 3.2 mm H/F X MAS probe. The spectra were processed using Bruker TopSpin 3.6.1 software.

2.6. Characterisation of Synthetic Fulvic Acid Solutions

Sample Preparation for Spectrophotometric Analyses: After separating artificial humic acids from the total reaction product, the SFS was further purified by centrifuging the solution to remove any excess colloidal particles. Following filtration, the sample was diluted 10 times.

FRAP Assay: The FRAP working solution was prepared by mixing 0.3 M sodium acetate (pH 3.6), 10 mM TPTZ (in 40 mM HCl), and 20 mM $FeCl_3$ solutions in a 10:1:1 ratio. The calibration working solution was prepared by dissolving Trolox in 96 % ethanol to achieve a concentration of 0.230 mg/mL. The calibration curve was established in the range of 4.16–45.7 µg/mL, yielding an R^2 value of 0.9996. For analysis, 50 µL of the sample, blank, or standard solution was transferred to a 96-well microplate, mixed with 150 µL of FRAP working solution, incubated at 37 °C for 30 minutes, and the absorbance was measured spectrophotometrically at 593 nm using a microplate reader (*Tecan Infinite 200 m nano+*, Austria). Samples were measured in quadruplicate.

Total Polyphenols: The calibration working solution was prepared by dissolving gallic acid in 96 % ethanol to a final concentration of 0.500 mg/mL. The calibration curve was established in the range of 13.5–203 µg/mL, yielding an R^2 value of 0.9993. For analysis, 50 µL of the sample, blank, or standard solution was transferred to a 96-well microplate, followed by the addition of 85 µL of FC working solution (0.2 M). The mixture was incubated at room temperature for 20 minutes, then 65 µL of 7.5 % Na_2CO_3 was added and incubated for another 10 minutes. The absorbance was measured spectrophotometrically at 765 nm. Samples were measured in quadruplicate.

DPPH Assay: The calibration working solution was prepared by dissolving Trolox in 96 % ethanol to a concentration of 0.230 mg/mL. The calibration curve was established in the range of 2.15–109 µg/mL, yielding an R^2 value of 0.99998. For analysis, 50 µL of the sample, blank, or standard solution was transferred to a 96-well microplate, mixed with 150 µL of DPPH working solution, and incubated for 30 minutes before measuring absorbance at 517 nm. Samples were measured in quadruplicate.

CUPRAC Assay: The CUPRAC working solution was prepared by mixing 10 mM $CuCl_2$, 7.5 mM neocuproine (in 96 % ethanol), and 1 M ammonium acetate (pH 7.0) in a 5:5:6 ratio. The calibration working solution was prepared by dissolving Trolox in 96 % ethanol to a concentration of 0.230 mg/mL. The calibration curve was established in the range of 6.40–230.0 µg/mL, yielding an R^2 value of 0.99996. For analysis, 50 µL of the sample, blank, or standard solution was transferred to a 96-well microplate, mixed with 150 µL of CUPRAC working solution, and incubated for 60 minutes before measuring absorbance at 450 nm. Samples were measured in quadruplicate.

Total Carbohydrates: The calibration working solution was prepared by dissolving glucose in deionized water to a concentration of 100 µg/mL. The calibration curve was established in the range of 1–75 µg/mL, yielding an R^2 value of 0.9989. For analysis, 1 mL of the sample was transferred to a glass test tube, mixed with 1 mL of a 5 % phenol solution, and incubated for 10 minutes. Then, 4 mL of concentrated H_2SO_4 was added, incubated for 20 minutes, and

the absorbance was measured spectrophotometrically at 490 nm using a spectrophotometer (*Shimadzu UV-1800*, Japan). Samples were measured in triplicate.

2.7. Statistical Analysis

A one-way ANOVA analysis was conducted to examine the effects of different temperatures and synthesis times on the total carbon transfer during hydrothermal humification. Following a significant ANOVA *p*-value result, Tukey's HSD (Honestly Significant Difference) post-hoc test was performed to identify which specific temperature and time groups differed significantly.

Data analysis was carried out using SPSS (Version 29, IBM Corp., Armonk, NY, USA). The one-way ANOVA was used to determine the overall effect of temperature and time on the hydrothermal humification synthesis process. Post-hoc comparisons were conducted using Tukey's HSD test to control for Type I error in multiple comparisons ($p < 0.001$; $\alpha = 0.05$; $n = 3$).

Pearson's correlation statistical analysis was performed using the open-source statistical software JASP (ver. 0.19.3.0) to calculate the correlation between each measured parameter.

3. Results and Discussion

3.1. Hydrothermal Humification Yield

It is paramount to assess the synthesis yield to produce artificial humic substances while varying synthesis temperature and time to maximise energy efficiency, in the meantime maximizing the yield of humic substances. Experimental data for carbon transfer from biomass to corresponding type of humic substance is provided in Table 1. Results show an increase of product yield for both artificial humic acids and fulvic acid solutions if the synthesis temperature is increased, particularly rapid increase is seen in the range from 155 °C to 185 °C. The same trend can be observed with increased synthesis duration. However, the dispersion in confidence interval for humic acid yield is significantly higher, which can be explained by hydrochar formation, which may lower the yield of AHAs. The diametrically opposite can be observed with formation of precursors, byproducts and fulvic acids when the process is conducted at the lowest 155 °C temperature, which can be explained with the fact that this is the base temperature necessary for HTH process to begin [8], and reaction product formation kinetics are erratic based on experimental data.

To assess the optimal conditions to achieve the highest yield of both AHAs and SFS, an ANOVA one-way test was conducted, using Tukey's Honestly Significant Difference test (Fig. 1).

It should be noted that Fig. 1 represents comparisons conducted using Tukey's HSD test to control for Type I error across multiple comparisons ($p < 0.001$; $\alpha = 0.05$; $n = 3$). To facilitate interpretation of statistical significance, the negative logarithm of all p-values ($-\log p$) was calculated, where the critical p-value is 0.001, corresponding to a value of 3 in the negative logarithm scale. If a value in the statistical significance matrix is greater than 3, it indicates that there is no statistically significant difference in the comparison of temperature or time matrices at the given temperature or time relative to the lower time or temperature, meaning the maximum outcome has been reached.

TABLE 1. EXPERIMENTAL CARBON TRANSFER DATA (MEAN ± CI) DURING HTH SYNTHESIS

T, °C	*t*, h	Total carbon transfer, mg C/g	SFS, mg C/g	AHA, mg C/g
155	2	258 ± 27	152 ± 106	106 ± 43
	4	291 ± 12	138 ± 153	153 ± 9
	9	329 ± 43	142 ± 187	187 ± 11
	14	337 ± 76	172 ± 189	189 ± 65
	24	302 ± 106	177 ± 170	170 ± 2
170	2	208 ± 28	135 ± 73	73 ± 10
	4	241 ± 28	161 ± 80	80 ± 25
	9	307 ± 30	185 ± 122	122 ± 42
	14	366 ± 3	208 ± 157	157 ± 20
	24	384 ± 45	240 ± 143	143 ± 12
185	2	319 ± 84	180 ± 22	139 ± 105
	4	368 ± 93	196 ± 40	172 ± 95
	9	380 ± 88	214 ± 26	166 ± 107
	14	423 ± 83	218 ± 15	204 ± 96
	24	423 ± 73	241 ± 17	182 ± 82
200	2	340 ± 56	181 ± 9	158 ± 47
	4	365 ± 81	204 ± 50	160 ± 43
	9	418 ± 85	221 ± 12	198 ± 92
	14	430 ± 76	235 ± 43	196 ± 37
	24	440 ± 51	249 ± 39	191 ± 90
215	2	319 ± 65	185 ± 27	134 ± 48
	4	380 ± 29	220 ± 10	160 ± 21
	9	439 ± 28	246 ± 22	193 ± 29
	14	437 ± 56	270 ± 26	167 ± 71
	24	446 ± 16	263 ± 13	183 ± 4
230	2	330 ± 26	185 ± 29	144 ± 10
	4	394 ± 117	225 ± 43	169 ± 114
	9	454 ± 55	242 ± 13	212 ± 55
	14	456 ± 89	258 ± 11	197 ± 100
	24	429 ± 99	254 ± 36	174 ± 110

Hydrothermal humification synthesis yield statistical significance matrix (-log *p*)

AHA yield vs synthesis duration

t, h	2	4	9	14	24
2		0.49	3.58	3.79	1.95
4	0.49			1.16	0.21
9	3.58	1.03		0.00	0.10
14	3.79	1.16	0.00		0.14
24	1.95	0.21	0.10	0.14	

SFS yield vs synthesis duration

t, h	2	4	9	14	24
2		0.53	2.29	5.06	6.89
4	0.53		0.31	1.98	3.43
9	2.29	0.31		0.37	1.22
14	5.06	1.98	0.37		0.07
24	6.89	3.43	1.22	0.07	

AHA yield vs synthesis temperature

T, °C	155	170	185	200	215	230
155		0.87	0.45	0.97	0.21	0.88
170	0.87		3.52	4.54	2.87	4.39
185	0.45	3.52		0.00	0.00	0.00
200	0.97	4.54	0.00		0.04	0.00
215	0.21	2.87	0.00	0.04		0.03
230	0.88	4.39	0.00	0.00	0.03	

SFS yield vs synthesis temperature

T, °C	155	170	185	200	215	230
155		1.18	4.40	5.76	9.17	8.44
170	1.18		0.62	1.37	3.93	3.33
185	4.40	0.62		0.01	0.90	0.58
200	5.76	1.37	0.01		0.31	0.14
215	9.17	3.93	0.90	0.31		0.00
230	8.44	3.33	0.58	0.14	0.00	

Fig. 1. ANOVA one-way significance test ($p < 0.001$; $\alpha = 0.05$; $n = 3$) for hydrothermal humification yield, expressed as $-\log p$. Blue represents synthesis temperature or time setting, green indicates the optimal conditions for desired product yield.

Results in Fig. 1 show that the synthesis temperature impact on yield for AHAs results in insignificant changes after reaching 185 °C; therefore, it is not necessary to increase the temperature to reach maximum yields. The same scenario was observed with SFS yield, resulting in no significant changes in carbon transfer after reaching 185 °C. However, there is a slight difference regarding the synthesis duration. For AHAs, the maximum yield is reached at 9 h, but there is a significant change when the residence time reaches 24 h, which can be explained by the fact that artificial humic acids start degrading after a prolonged synthesis. On other hand, SFS yield peaks at 14 h residence time, and contrary to AHAs, the yield continues to grow, which indicates the continuous formation of low molecular substances and fulvic acids.

3.3. Physico-Chemical Characterisation of Artificial Humic Acids

To compare the degree of humification, relative molecular weight, and the qualitative properties of chromophore groups in the obtained artificial humic acids, molecular absorption spectra were recorded in the range of 220–700 nm. To identify empirical trends in structural changes within the humic acid synthesis design, molecular absorption spectra were recorded for humic acids synthesized for 14 hours at different temperatures, with the results presented in Fig. 2.

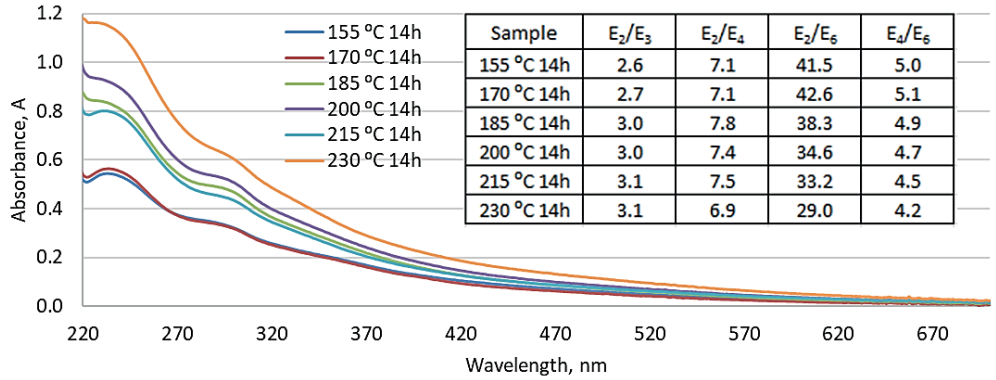

Sample	E_2/E_3	E_2/E_4	E_2/E_6	E_4/E_6
155 °C 14h	2.6	7.1	41.5	5.0
170 °C 14h	2.7	7.1	42.6	5.1
185 °C 14h	3.0	7.8	38.3	4.9
200 °C 14h	3.0	7.4	34.6	4.7
215 °C 14h	3.1	7.5	33.2	4.5
230 °C 14h	3.1	6.9	29.0	4.2

Fig. 2. Molecular absorption spectra of artificial humic acids derived from spruce greenery depending on the synthesis temperature at a constant synthesis time of 14 hours.

The absorption spectra clearly show a general increase in absorption as the synthesis temperature is increased, especially in the UV region (220–400 nm), which is associated with the formation of aromatic and conjugated chromophore groups [16]. The sample synthesized at 230 °C shows the highest absorption, reflecting the most intense humification and structural condensation, while lower temperatures (155 °C and 170 °C) show lower overall absorption, indicating simpler and less aromatic molecular structures.

The E_2/E_3 ratio increases from 2.6 at 155 °C to 3.1 at temperatures of 200 °C or higher, indicating a transition to larger molecular weights and more complex aromatic structures with increasing temperature [17]. Similarly, the E_2/E_4 ratio peaks at 185 °C at 7.8, indicating the lowest degree of aromaticity, but then slightly decreases at higher temperatures, such as 6.9 at 230 °C, suggesting further condensation and stabilization of aromatic structures. The E_2/E_6 and E_4/E_6 ratios show a decreasing trend with increasing synthesis temperature, starting with the highest values of 41.5 and 5.0 at 155 °C, respectively, indicating simpler and less condensed structures, transitioning to lower values of 29.0 and 4.2 at 230 °C, indicating greater aromatic condensation and humification.

These results prove that increasing the temperature enhances the aromaticity and structural complexity of HS, and higher temperatures promote the formation of more condensed and stable aromatic structures. The data indicate that synthesis temperature is a crucial factor that can be used to tailor HS for specific applications, with higher temperatures yielding more refractory and functionally diverse materials. Similarly, the experiment was done to examine the effect of synthesis duration, using humic acids synthesized at 200 °C with varying treatment times. The results are shown in Fig. 3.

Results in Fig. 3 reveal that the E_2/E_3 ratio remains relatively unchanged at values of 3.0–3.1 when the synthesis duration is 4 hours or longer, highlighting a consistent molecular mass and aromatic complexity with longer synthesis times. However, the 2-hour sample shows a lower E_2/E_3 ratio of 2.6, indicating less aromaticity and structural development. Similarly, the E_2/E_4 ratio is highest during the 24-hour synthesis, reflecting increased aromaticity and conjugation, while decreasing the synthesis temperature leads to humic acids with significantly lower values, corresponding to simpler structures. The E_2/E_6 and E_4/E_6 ratios gradually decrease with longer synthesis times, with the lowest values occurring during the 24-hour synthesis, indicating more efficient aromatic condensation.

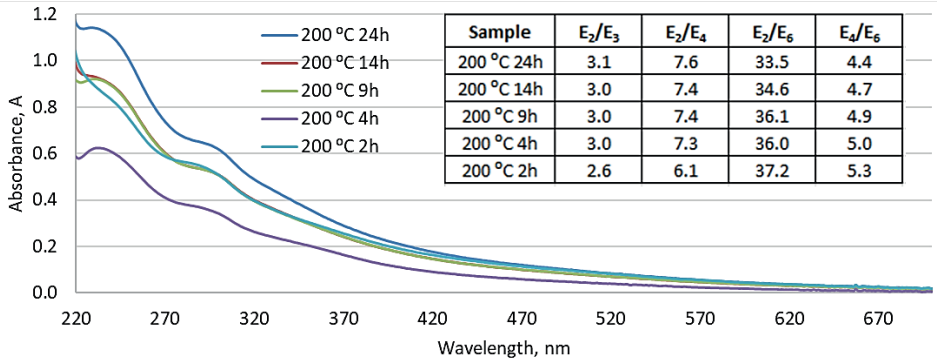

Sample	E_2/E_3	E_2/E_4	E_2/E_6	E_4/E_6
200 °C 24h	3.1	7.6	33.5	4.4
200 °C 14h	3.0	7.4	34.6	4.7
200 °C 9h	3.0	7.4	36.1	4.9
200 °C 4h	3.0	7.3	36.0	5.0
200 °C 2h	2.6	6.1	37.2	5.3

Fig. 3. Molecular absorption spectra of artificial humic acids derived from spruce greenery depending on the synthesis time at a constant synthesis temperature of 200 °C.

These trends show that longer synthesis times promote the gradual development of more complex, condensed, and aromatic humic acid structures, making synthesis time an important factor when tailoring AHAs for specific applications; however, synthesis temperature has a more notable impact on the formation of highly condensed AHAs.

To better understand the dynamics of functional groups in the humic acids obtained from the humification process, FTIR spectra were recorded. First, the impact of temperature on the dynamics of the functional groups in AHAs was analysed, and the FTIR spectra are shown in Fig. 4, where the transmittance for each sample is artificially shifted to prevent signal overlap and is defined as relative.

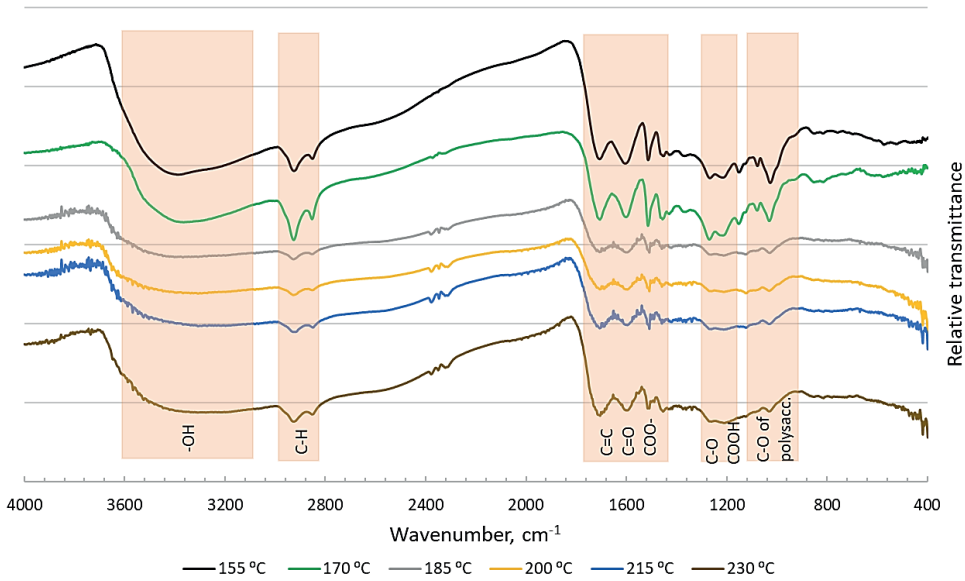

Fig. 4. FTIR spectra of artificial humic acids derived from spruce greenery biomass at different temperatures at a constant 14 h synthesis time.

Fig. 4 shows the FTIR spectra of artificial humic acids synthesized at temperatures ranging from 155 °C to 230 °C over a constant 14-hour period, illustrating the structural development of these substances as the reaction temperature increases. The broad O-H stretching band (3200–3600 cm^{-1}) decreases in intensity at higher temperatures, reflecting dehydration and condensation reactions that reduce the content of hydroxyl groups. Similarly, the C-H stretching bands (2800–3000 cm^{-1}), indicative of aliphatic structures, decrease with increasing temperature, pointing to the breakdown of aliphatic chains and a shift towards more aromatic and condensed molecules. The aromatic C=C stretching band region (1500–1600 cm^{-1}) becomes more pronounced at higher temperatures, indicating an increase in aromaticity and structural condensation. The C=O stretching band (~1700 cm^{-1}) sharpens and intensifies, suggesting the formation and stabilization of carbonyl groups due to oxidation and condensation reactions. The carboxylate COO^- stretching bands (1200–1400 cm^{-1}) decrease in intensity, indicating decarboxylation processes, while the C-O stretching and phenolic O-H bending bands (~1000–1300 cm^{-1}) weaken, reflecting the loss of hydroxyl groups and carbohydrate-related groups as aromaticity increases. The aromatic C-H bending (~700–900 cm^{-1}) intensifies at higher temperatures, further confirming the formation of condensed polyaromatic structures [18].

Overall, the data reveal a clear progression with increasing synthesis temperature. At lower temperatures, more aliphatic and hydroxyl group properties are preserved, while at higher temperatures, humic acids exhibit increased aromaticity, condensation, and structural reinforcement, with the highest level of humification observed at 230 °C. To understand the dynamics of synthesis time, FTIR spectra were recorded for humic acids synthesized at 200 °C under varying synthesis durations (Fig. 5).

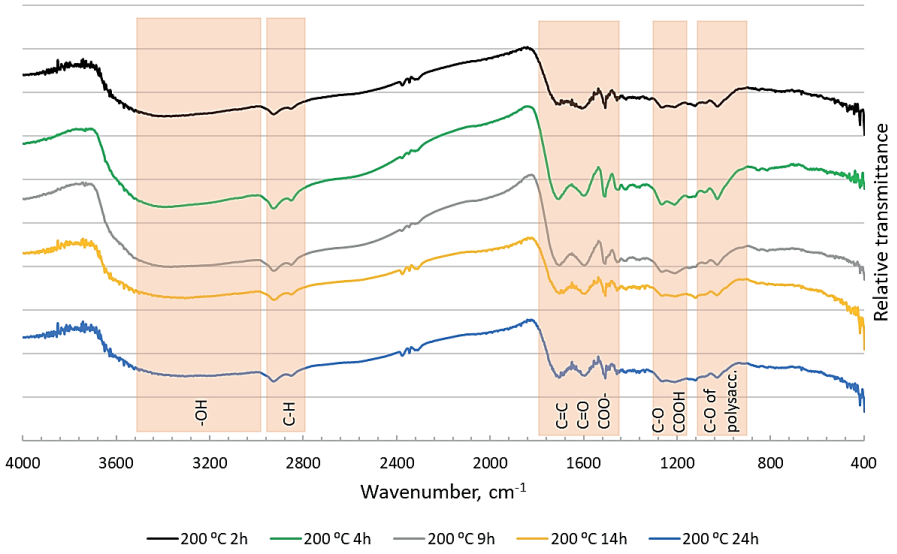

Fig. 5. FTIR spectra of artificial humic acids derived from spruce greenery biomass at different synthesis residence times at a constant 200 °C synthesis temperature.

The FTIR spectra visualized in Fig. 5 highlight the structural changes in artificial humic acids synthesized at 200 °C with varying reaction durations (2 h, 4 h, 9 h, 14 h, and 24 h). After 2 hours, the spectrum is dominated by a broad -OH stretching peak (3200–3600 cm^{-1}),

indicating hydroxyl groups from alcohols, phenols, or water, along with a strong aliphatic C-H stretching band (2800–3000 cm^{-1}), signifying the presence of aliphatic chains. The signals for aromatic C=C (1500–1600 cm^{-1}) and carbonyl C=O (~1700 cm^{-1}) are weak, suggesting minimal condensation and oxidation.

As the reaction continues to 4 hours, the -OH and C-H peaks begin to weaken, indicating dehydration and a reduction in aliphatic content, while the aromatic C=C and C=O vibrations intensify, reflecting the formation of aromatic rings and oxidized functional groups. By 9 hours, aliphatic signals have significantly decreased, and aromatic and carbonyl peaks dominate, indicating increasing aromaticity and oxidation, consistent with the polymerization and humification process. Peaks at ~1400 cm^{-1} (COO^- stretching) and 1200–1300 cm^{-1} (C-O stretching) increase in intensity, suggesting the formation of carboxylic acids, esters, or phenol groups.

After 14 hours, the spectrum is characterized by strong aromatic and carboxyl group signals, with fewer aliphatic features, marking a more advanced humification stage. At 24 hours, the material becomes highly aromatic and oxidized, with pronounced aromatic (C=C) and carbonyl (C=O) peaks and minimal -OH and polysaccharide-related signals (~1000–1100 cm^{-1}), indicating extensive polymerization, dehydration, and oxidation. However, changes in the aromatic C-H bending region (700–900 cm^{-1}) are not significantly affected by increased temperature.

Although synthesis time plays a role in humic acid formation, synthesis temperature is more critical, as evidenced by the more intense spectral changes at higher temperatures. To further explore the impact of temperature on the functional group dynamics in hydrothermally humified humic acids, ^{13}C-CPMAS-NMR spectra were recorded (Fig. 6).

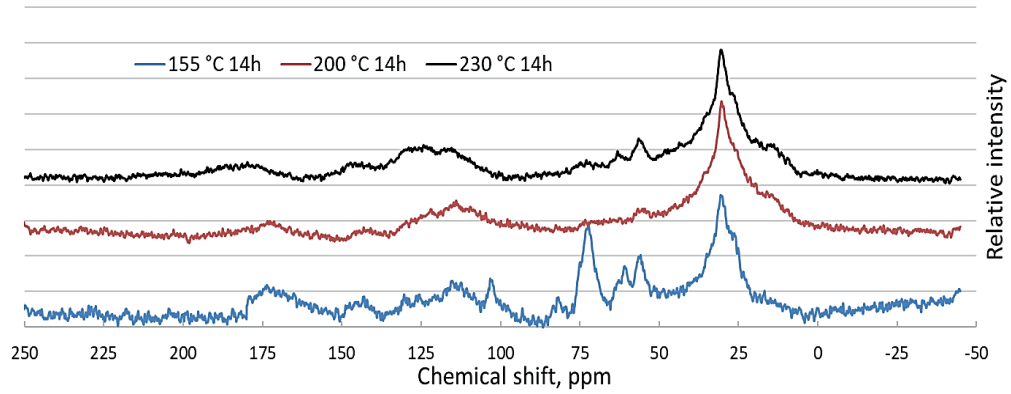

Fig. 6. ^{13}C-CPMAS-NMR spectra of artificial humic acids synthesized for 14 hours at 155, 200, and 230 °C.

The experimental ^{13}C-CPMAS-NMR spectra of artificial humic acids visualized in Fig. 6 correspond to AHA obtained in the study, with synthesis temperatures selected at 155 °C (lowest), 200 °C (intermediate), and 230 °C (highest) to provide additional insights into the dynamics of AHA functional groups depending on the synthesis temperature. Additionally, the relative percentage distribution of these AHA functional groups in the material was calculated based on peak area (Table 2).

TABLE 2. DISTRIBUTION OF CARBON FUNCTIONAL GROUPS IN ^{13}C-CPMAS-NMR SPECTRUM OF ARTIFICIAL HUMIC ACIDS [19]

AHA	220–190 ppm	190–160 ppm	160–140 ppm	140–110 ppm	110–90 ppm	90–60 ppm	60–50 ppm	50–0 ppm	Aliphaticity*	Aromaticity**
	C=O	>CO – O, N	C_{Ar} – O, N	C_{Ar}	OC-O, N	C-O, N	OCH_3	CH_n	%	%
155 °C	2	11	5	12	6	17	8	39	71	17
200 °C	3	7	2	12	13	9	5	48	75	15
230 °C	6	8	5	17	4	10	6	44	64	22

Note *corresponds to total aliphaticity of the structure in range of 0–110 ppm; ** corresponds to total aromaticity of the AHA structure in range of 110–160 ppm.

The ^{13}C-CPMAS-NMR spectra (Fig. 6) and functional group distribution data (Table 2) illustrate the structural dynamics of AHAs obtained through the hydrothermal humification process at 155 °C, 200 °C, and 230 °C for 14 hours.

At 155 °C, the humic acids are characterized by a high proportion of aliphatic carbon (0–50 ppm, 39 %), a significant carbohydrate content (60–90 ppm, 17 %), and methoxy groups (50–60 ppm, 8 %), reflecting the early stages of humification, dominated by lignin- and polysaccharide-derived precursors. These components indicate relatively unmodified biomass, preserved with limited aromatic condensation or oxidation. The carbohydrate-rich fraction (60–90 ppm) at this stage highlights the preservation of polysaccharides or their fragments, while the methoxy signal (50–60 ppm) indicates the presence of lignin-like structures. As the temperature increases to 200 °C, a more pronounced degree of humification becomes evident. The aliphatic fraction reaches its maximum (0–50 ppm, 48 %), while carbohydrates decrease significantly (60–90 ppm, 9 %), and aromatic carbons with alkyl substituents (110–140 ppm, 13 %) show a slight increase. This suggests a transition from polysaccharide and lignin-rich precursors to partially condensed structures, driven by hydrolysis and dehydration reactions. The reduction in methoxy groups to 5 % in the range of 50–60 ppm indicates degradation of lignin-derived structures, while a slight increase in oxidized functional groups such as carboxyl and ester groups (160–190 ppm, 7 %) suggests oxidation of aliphatic chains and the formation of more functionalized compounds. At 230 °C, the humic acids exhibit progressive humification, characterized by a significant increase in aromatic content (110–160 ppm, 22 %) and oxidation levels, with carboxylic acid and ester functional groups reaching 8 %, and ketone and quinone carbons (190–220 ppm) increasing to 6 %. The aliphatic fraction decreases (0–50 ppm, 44 %) compared to 200 °C, reflecting the condensation of thermally unstable aliphatic structures into more stable aromatic and oxidized forms via condensation and oxidation reactions. The near-complete loss of carbohydrates (4 %) and methoxy groups (6 %) suggests the decomposition of polysaccharide and lignin residues, while the enrichment of oxygen or nitrogen-associated aromatic carbons (140–160 ppm, phenols and aromatic ethers) indicates an increasing degree of humification.

The observed trends reflect the gradual degradation of labile components and accumulation of thermally stable structures. Increasing temperature accelerates the humification process, producing artificial humic acids at 230 °C that exhibit properties characteristic of natural humic acids, including high aromaticity, functional group diversity, and oxidation. Reaction temperatures reaching 230 °C also come with intensive formation of free radicals, explored in Fig. 7.

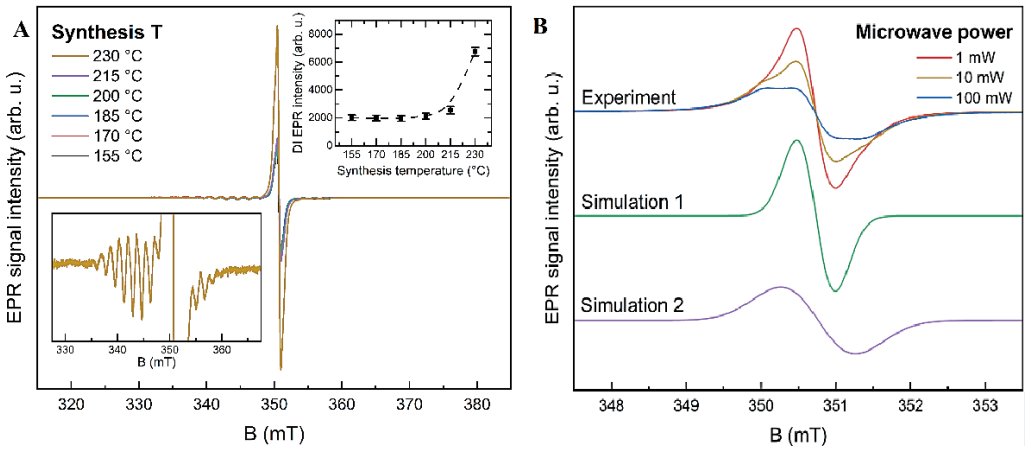

Fig. 7. EPR spectra (10 mW microwave power) of AHA samples after synthesising at different temperatures (A). Inset (lower left corner): magnified EPR spectrum of the HA sample synthesised at 230 °C; inset (upper right corner): double integrated (DI) EPR signal intensity in the 348–357 mT range as a function of synthesis temperature. EPR spectra simulations of the AHA sample synthesised at 230 °C (B).

Fig. 7 shows the EPR spectra (A) of the investigated AHA samples after synthesis at different temperatures. A symmetric signal at 351 mT (g = 2.00) is observed in all samples. The intensity of this signal increases with higher synthesis temperatures, reaching an approximately trifold increase at 230 °C compared to 155 °C, which can be explained with increase of quinone structure relative concentration represented in Table 2 (220–190 ppm, C=O). In addition, a smaller intensity signal with an intricate hyperfine (HF) structure is present, with comparable signal intensities for all samples. Similar HF patterns have been associated with the 4.9-dihydroxyperylene-3.10-quinone (DHPQ) structure [20].

EPR spectra dependence on microwave power (Fig. 7, B) indicates that the g = 2.00 signal is composed of two overlapping components. EPR spectra parameters for these components are estimated as follows: g = 2.0034 ± 0.0005 with a peak-to-peak linewidth of 0.5 ± 0.1 mT (Simulation 1) and g = 2.0033 ± 0.0005 with a peak-to-peak linewidth of 1.0 ± 0.1 mT (Simulation 2). Similar EPR signals have been detected and described by several authors, and they are suggested to arise from semiquinone-type free radicals [21], [22].

3.4. Characterisation of Synthetic Fulvic Acid Solutions

Solutions of low-molecular-weight fulvic acids and other byproducts, which form in tandem with artificial humic acids as the primary product, have been studied to a limited extent. However, given that significant carbon transfer from biomass occurs in the HTH process, it is important to understand which intermediates or byproducts remain after synthesis, as well as the dynamics and structural composition of these substances, considering that fulvic acids are the second major product.

Based on a literature review of the HTH mechanism, it is known that lignin primarily breaks down into smaller monomers, forming low-molecular-weight polyphenol-like byproducts, while the decomposition of cellulose and hemicellulose may leave behind unreacted mono-, di-, or oligosaccharides with various structures [10], [23].

To determine the dynamics of intermediate residues, a spectrophotometric analysis of total carbohydrates and polyphenols was conducted (Fig. 8).

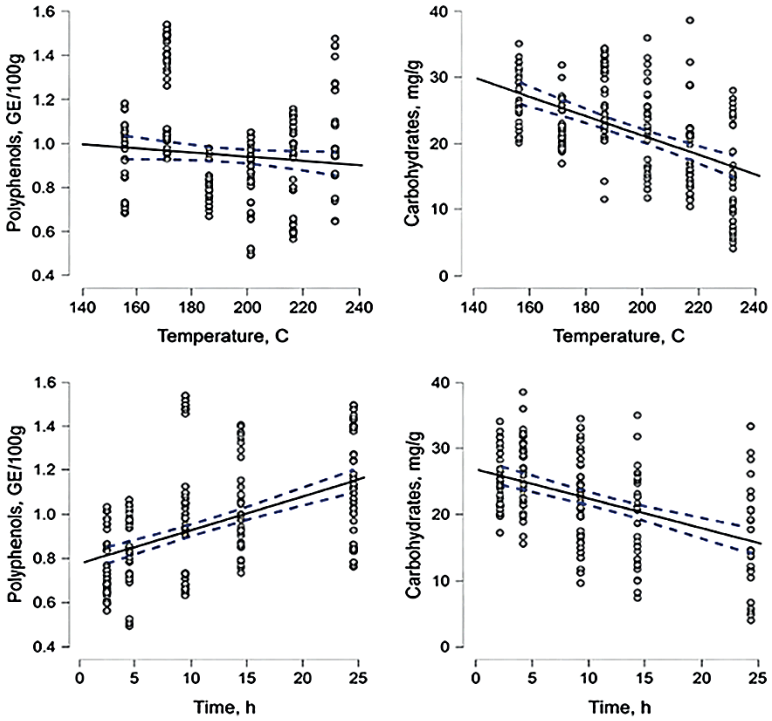

Fig. 8. Total carbohydrate and polyphenol content in the liquid phase and their dynamics depending on synthesis temperature and time in synthesis byproducts. Total carbohydrates are expressed in mg per 1 gram of biomass and total polyphenols are expressed as gallic acid equivalents per 100 g of biomass.

Fig. 8 displays four scatter plots illustrating the relationships between time, temperature, and the concentrations of total carbohydrates and polyphenols, which form as byproducts of the hydrothermal humification process.

The polyphenol content tends to increase over time. A positive correlation is observed, as indicated by the upward trend of the regression line and the clustering of data points. This suggests that a longer reaction time promotes polyphenol formation under the given conditions. In contrast, the carbohydrate content shows a negative correlation with time. The downward trend of the regression line indicates that prolonged reaction times lead to a gradual degradation or transformation of carbohydrates into other compounds. A clear negative correlation is observed between temperature and carbohydrate content. As the temperature increases, the carbohydrate concentration decreases, suggesting that higher temperatures likely promote carbohydrate decomposition during the humification process. The relationship between temperature and polyphenol content is less pronounced, showing a slightly negative trend. This indicates that while temperature may have some influence, other factors such as reaction time or kinetics may play a more significant role in determining polyphenol content.

Overall, the data suggest that reaction time primarily drives polyphenol synthesis, while higher temperatures and prolonged reaction times promote carbohydrate degradation in the hydrothermal humification process. Although the total content of unreacted total carbohydrate and polyphenol-like substances in SFS is low, for carbohydrates reaching 39.6 mg/g and polyphenol concentrations reaching up to 1.5 GE/100 g, the dynamics of their formation are explored. Furthermore, low-molecular byproduct antioxidant and antiradical activity dynamics are explored in Fig. 9.

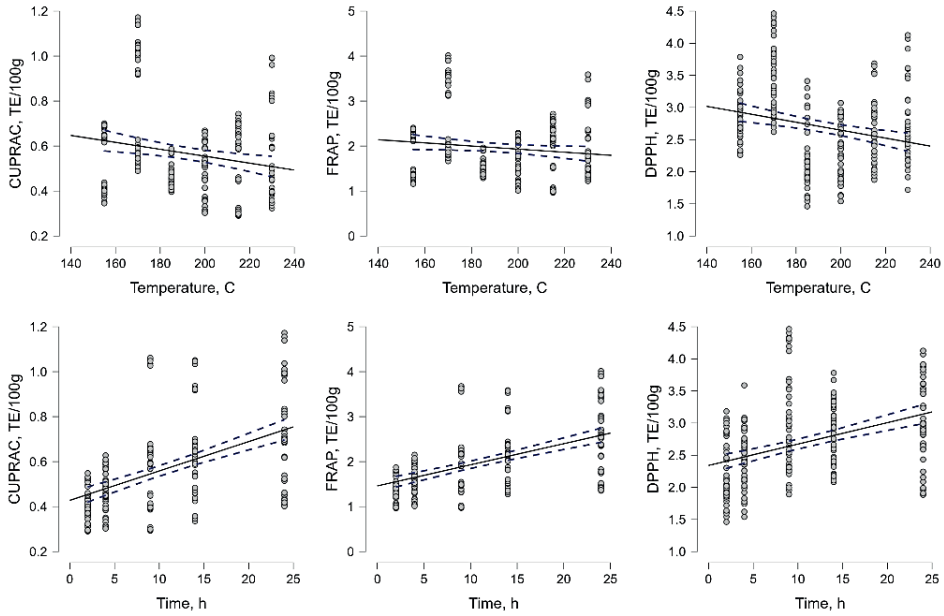

Fig. 9. The dynamics of antioxidant activities (FRAP, CUPRAC) and antiradical activity (DPPH) depending on the synthesis temperature and time in the synthesis by-products.

The correlation graphs in Fig. 9 illustrate the dynamics of antioxidant activities (FRAP and CUPRAC) and antiradical activity (DPPH) in the synthetic fulvic acid solutions isolated from humic acids, considering the synthesis temperature (155–230 °C) and reaction time (2–24 h).

Regarding temperature, FRAP values show a slight negative trend as the temperature increases, indicating that the effect of higher temperatures on by-product formation during synthesis is minimally negative. In contrast, both DPPH and CUPRAC activities show a clear negative correlation with temperature, suggesting that elevated temperatures disrupt the structure of thermally sensitive antioxidant compounds or change important activity characteristics, such as functional groups or solubility. Specifically, higher temperatures seem to reduce the ability of these residual products to neutralize radicals or decrease the concentration of copper (II) ions, reflecting a loss of active antioxidant compounds. On the other hand, reaction time positively affects all measured activities. FRAP values increase with longer reaction times, indicating the gradual formation or stabilization of antioxidants in the residual liquids. Similarly, DPPH activity improves with longer reaction times, indicating enhanced radical neutralization abilities as the humification process continues. CUPRAC activity also increases over time, reflecting an increasing ability to reduce copper (II) ions, likely due to the accumulation of active by-products as the reaction progresses. These results emphasize that temperature and reaction time have different, yet complementary, effects on the antioxidant and antiradical properties of the by-products.

While excessively high temperatures can degrade active compounds, longer reaction times improve antioxidant development and stabilization, highlighting the need to optimize both parameters to achieve maximum activity in hydrothermal humification processes. It should be noted that both antioxidant activity and antiradical activity are generally low, reaching ~4 g Trolox equivalents per 100 g of biomass weight for FRAP; ~1.2 g Trolox equivalents per 100 g of biomass weight and, at most, ~4.5 g gallic acid equivalents per 100 g of dry

biomass weight. These low values correlate well with the previously determined polyphenol content.

4. CONCLUSIONS

The study highlights the potential of hydrothermal humification as a sustainable end-of-waste strategy for valorising forestry logging side streams, specifically extracted spruce greenery biomass, into artificial humic substances. Key findings emphasize that HTH offers a climate-neutral pathway to replace peat-derived humic substances, aligning with circular bioeconomy principles and reducing dependence on slowly renewable fossil resources.

Optimal conditions for maximizing artificial humic acid yields were identified at 185 °C with a 9-hour synthesis duration, while synthetic fulvic acids and other low molecular by-products continued forming up to 14 hours. For example, Shao *et al*. [18] reported a total of 28.3 % artificial humic acid yield at 260 °C using corn stalk as biomass feed, which is close to the yield in this study. However, Han *et at*. [24] obtained a AHA yield of 40.3 % using corn-straw digestate with reported optimal temperature of 156 °C and 2-hour synthesis time. Higher temperatures and prolonged synthesis enhanced aromaticity and structural complexity, leading to the formation of more stable humic substances. Analytical techniques such as UV-Vis, FTIR, EPR, and ^{13}C-CPMAS-NMR confirmed the development of condensed aromatic structures, increased carbon retention, and the progressive degradation of aliphatic content with rising temperature and synthesis time. The evolution of optical indices with temperature and time increase is fully consistent with the behaviour of AHAs produced from other lignocellulosic feedstocks. Sui et al. [8] observed a similar increase in UV absorbance and decrease in E_4/E_6 for AHAs obtained from vegetable wastes, which they attributed to progressive aromatic condensation and growth of conjugated chromophore domains. Similar findings are reported by Ischia *et al*. [25], where ^{13}C-CPMAS-NMR patterns are observed in AHAs that are synthesised from lignin and cellulose, notably the dominant aliphatic region of <60 ppm and relative proportion of 67 %. Their findings also note a distinct signal in 170–110 ppm domain that is characteristic for polyaromatic structures. Furthermore, FTIR spectra in Ischias' study show that AHAs from both cellulose and lignin share a common condensed fingerprint – an aromatic C=C band around 1615 cm^{-1}, methoxy related C-H bands at ~1460 and 1425 cm^{-1}, aliphatic C-H stretching near 2900 cm^{-1}, and broad O-H (3000–3500 cm^{-1}) plus C=O/COOH (1695–1700 cm^{-1}) and C-O (1030–1200 cm^{-1}) bands respectively. Although, caution must be taken when applying temperatures over 200 °C, because of free radical formation.

The study also revealed that by-products, such as polyphenol-like and carbohydrate-like structures (including furfuroles), exhibit distinct dynamics – polyphenolic content increased with synthesis duration, while carbohydrate-like substance content declined, indicating progressive decomposition. Antioxidant and antiradical activities correlated positively with reaction time, suggesting the formation of bioactive compounds during prolonged synthesis. It should be noted that both the total polyphenols (Folin-Ciocalteu) and total carbohydrate (phenol-sulfuric acid) assays used here provide operational rather than compound-specific quantification. The Folin-Ciocalteu reagent responds to a wide range of reducing and antioxidant functional groups, including some non-phenolic moieties, while the phenol-sulfuric acid method detects all carbohydrate-like structures that can be dehydrated under strongly acidic conditions, including saccharides covalently bound to the humic matrix. In the present work, we therefore focus on the clear decrease in carbohydrate-like content and

the moderate increase in phenolic-like reactivity with reaction time, which together indicate progressive incorporation of labile saccharides into more condensed structures while a fraction of phenolic patterns remains available in the SFS.

In conclusion, HTH is an efficient method for converting forestry biomass waste into valuable humic substances, presenting a sustainable alternative to peat extraction. Further research should focus on optimizing process parameters, scaling up the technology, and exploring practical applications of artificial humic substances in agriculture and environmental remediation. This approach supports climate-neutral strategies, reduces greenhouse gas emissions, and promotes circular bioeconomy practices in forestry management.

ACKNOWLEDGEMENT

This research was funded by the Rural Support Service Republic of Latvia project "Full-cycle processing of green biomass from skewers to produce high-value feedstocks for the chemical and pharmaceutical industries" (Nr: 23-00-A01612-000007)

REFERENCES

[1] European Commission. A sustainable bioeconomy for Europe: strengthening the connection between economy, society and the environment. Brussels, 2018.

[2] The European Green Deal. Striving to be the first climate-neutral continent. [Online]. [Accessed 13.03.2025]. Available: https://commission.europa.eu/strategy-and-policy/priorities-2019-2024/european-green-deal_en.

[3] Latvian Peat Association. Peat extraction and GHG emissions, 2022. [Online]. [Accessed 18.03.2025]. Available: https://www.latvijaskudra.lv/en/Interesting_information/ghg_emissions/

[4] Pajtík J., Konôpka B., Lukac M. Biomass Functions and Expansion Factors in Young Norway Spruce (*Picea abies* [L.] Karst) Trees. *Forest Ecology and Management* 2008:256(5):1096–1103. https://doi.org/10.1016/J.FORECO.2008.06.013

[5] Forestry in 2021. Official statistics of Latvia. [Online]. [Accessed 13.05.2025]. Available: https://stat.gov.lv/en/statistics-themes/business-sectors/forestry/publications-and-infographics/10963-forestry-2021.

[6] Mezulis M., Arbidans L., Millere L. L., Lauberts M., Grinfelds U., Klavins M. Green Chemistry Approaches for Processing of Coniferous Needles and Greenery to Implement Circular Bioeconomy Concepts in Forestry. *Environmental and Climate Technologies* 2025:29(1):97–133. https://doi.org/10.2478/rtuect-2025-0007

[7] Shi Y., Matsunaga T., Saito M., Yamaguchi Y., Chen X. Comparison of global inventories of CO_2 emissions from biomass burning during 2002–2011 derived from multiple satellite products. *Environmental Pollution* 2015:206:479–487. https://doi.org/10.1016/j.envpol.2015.08.009

[8] Sui W., Li S., Zhou X., Dou Z., Liu R., Wu T., Jia H., Wang G., Zhang M. Potential Hydrothermal-Humification of Vegetable Wastes by Steam Explosion and Structural Characteristics of Humified Fractions. *Molecules* 2021:26(13):3841. https://doi.org/10.3390/molecules26133841

[9] Hu Z.-T., Huo W., Chen Y., Zhang Q., Hu M., Zheng W., Shao Y., Pan Z., Li X., Zhao J. Humic Substances Derived From Biomass Waste During Aerobic Composting and Hydrothermal Treatment: A Review. *Frontiers* in Bioengineering and Biotechnology 2022:10. https://doi.org/10.3389/fbioe.2022.878686

[10] Zhu Y., Cao Y., Fu B., Wang C., Shu S., Zhu P., Wang D., Xu H., Zhong N., Cai D. Waste Milk Humification Product Can Be Used as a Slow Release Nano-Fertilizer. *Nature Communications* 2024:15:128. https://doi.org/10.1038/s41467-023-44422-5

[11] Li X., Zhi Y., Jia M., Wang X., Tao M., Wang Z., Xing B. Properties and Photosynthetic Promotion Mechanisms of Artificial Humic Acid Are Feedstock-Dependent. *Carbon Research* 2024:3:4. https://doi.org/10.1007/s44246-023-00085-x

[12] Zhao B.C., Wang Y., Ma L., Deng Y., Xu Z. Adjusting pH of the Secondary Composting Materials to Further Enhance the Lignocellulose Degradation and Promote the Humification Process. *Social Science Research Network* 2023:15(1):9032. https://doi.org/10.3390/su15119032

[13] Čabalová I., Bélik M., Kučerová V., Jurczyková T. Chemical and Morphological Composition of Norway Spruce Wood (*Picea abies*, L.) in the Dependence of Its Storage. *Polymers* 2021:13(10):1619. https://doi.org/10.3390/polym13101619

[14] Kļaviņš M., Ansone-Bērtiņa L., Arbidans L., Kļaviņš L. Biomass waste processing into artificial humic substances. *Environmental and Climate Technologies* 2021:25(1):631–639. https://doi.org/10.2478/rtuect-2021-0047

[15] Stoll S., Schweiger A. EasySpin, a comprehensive software package for spectral simulation and analysis in EPR. *Journal of Magnetic Resonance* 2006:178:42–55. https://doi.org/10.1016/j.jmr.2005.08.013

[16] Senese G. S., Martin-Neto L., Villas-Boas P. R., Nicolodelli G., Milori D. M. Laser-based spectroscopic methods to evaluate the humification degree of soil organic matter in whole soils: A review. *Journal of Soils and Sediments* 2018:18(4):1292–1302. https://doi.org/10.1007/s11368-016-1539-6

[17] Rosset J. S., Tavares O. C. H., Pereira M. G., do Carmo Lana M., Schiavo J. A., Barros Ozório J. M., Lima S. M. Chemical and Spectroscopic Characteristics of Humic Acids Under No-Tillage and Forest Systems. *Communications in Soil Science and Plant Analysis* 2023:55(6):796–813. https://doi.org/10.1080/00103624.2023.2277415

[18] Shao Y., Bao M., Huo W., Ye R., Liu Y., Lu W. Production of artificial humic acid from biomass residues by a non-catalytic hydrothermal process. *Journal of Cleaner Production* 2022:335:130302. https://doi.org/10.1016/j.jclepro.2021.130302

[19] He Z.-Q., Cao X.-Y., Mao J.-D., Ohno T., Waldrip H. M. Analysis of Carbon Functional Groups in Mobile Humic Acid and Recalcitrant Calcium Humate Extracted from Eight US Soils. *Pedosphere* 2013:23(6):705–716. https://doi.org/10.1016/S1002-0160(13)60063-6

[20] Watanabe A., McPhail D. B., Maie N., Kawasaki S., Anderson H. A., Cheshire M. V. Electron spin resonance characteristics of humic acids from a wide range of soil types. *Organic Geochemistry* 2005:36(7):981–990. https://doi.org/10.1016/j.orggeochem.2005.03.002

[21] Polewski K., Sławińska D., Sławiński J., Pawlak A. The effect of UV and visible light radiation on natural humic acid EPR spectral and kinetic studies. *Geoderma* 2005:126(3–4):291–299. https://doi.org/10.1016/j.geoderma.2004.10.001

[22] Barriquello M. F., Da S., Saab C., Filho N. C., Martin-Neto L. Electron Paramagnetic Resonance Characterization of a Humic Acid-Type Polymer Model. *Journal of the Brazilian Chemical Society* 2010:21(12). https://doi.org/10.1590/S0103-50532010001200018

[23] Sutradhar S., Fatehi P. Latest Development in the Fabrication and Use of Lignin-Derived Humic Acid. *Biotechnology for Biofuels and Bioproducts* 2023:16:38. https://doi.org/10.1186/s13068-023-02278-3

[24] Han S-Z., Zhang B-T., Wang M-Q., Guo R-B., Fu S-F. Optimization of alkaline hydrothermal treatment for humic acids production from corn straw digestate using the response surface methodology. *Journal of Environmental Chemical Engineering* 2024:12(2):112465. https://doi.org/10.1016/j.jece.2024.112465

[25] Ischia G., Marzban N., Schmidt J. Volikov A. Transitioning from hydrothermal carbonization to humification for producing artificial humic substances. *Bioresource Technology* 2026:439:133306. https://doi.org/10.1016/j.biortech.2025.133306